Supporting Information

1. Zeolite Elimination Process

A critical step in Zeolite-Templated Carbon (ZTC) synthesis is the effective removal of the inorganic zeolite framework. Zeolites are ceramic aluminosilicates (SiO_4– AlO_4) that require rigorous conditions to break the $Si-O$ and $Al-O$ bonds. In this work, the elimination was achieved via a two-step leaching process. First, a desilication step was performed using $2\ M\ NaOH$ at $80°C$ for $2\ h$. This was followed by a dealumination step utilizing $1\ M\ HCl$ at room temperature (RT) for $2\ h$ [1].

The complete removal of the zeolite was confirmed by thermogravimetric analysis (TGA) and X-ray diffraction (XRD), as shown in Figure S1. TGA was performed in air up to $800°C$ to combust the organic phase. The residual mass, attributable to the inorganic phase, decreased from 83% to 0% after the washing process. XRD patterns collected before the leaching process were similar to those of the pristine zeolite powder; however, post-leaching diffractograms exhibited only the broad reflections characteristic of amorphous carbon.

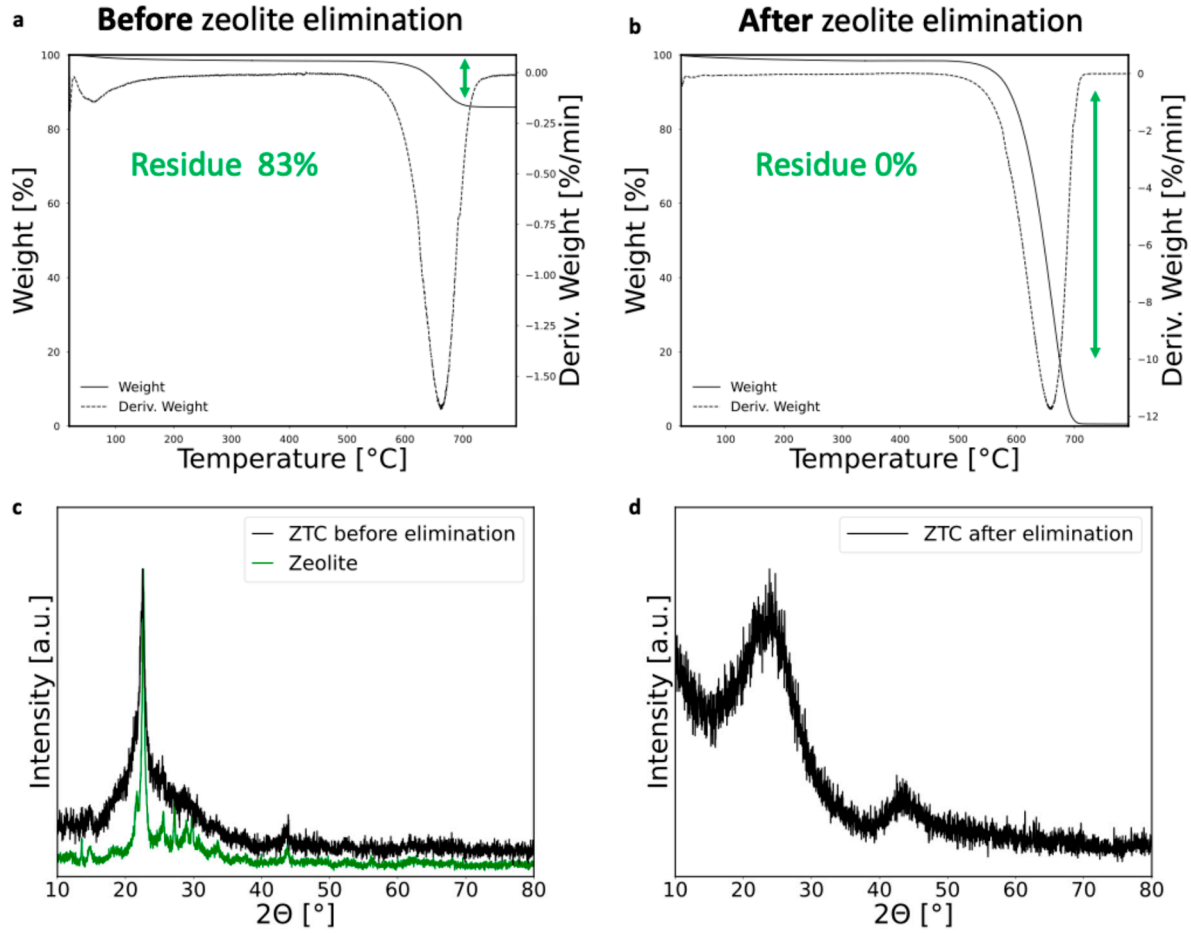


Figure S1. Proof of zeolite template removal before and after leaching process: **(a–b)** thermogravimetric analysis (TGA) profiles in air up to 800 °C; **(c–d)** X-ray diffraction (XRD) patterns.

2. Experimental Data Processing

Data processing was performed using a custom Python-based routine (v3.9) utilizing the SciPy and Pandas libraries.

2.1. X-ray Diffraction

The structural parameters were determined using the Bragg and Scherrer equations as described in the main text [2]. To define precise peak positions and broadening, the (002) and (10) reflections were fitted with a Gaussian distribution function:

$$f(x) = a \cdot \exp\left(-\frac{(x-x_0)^2}{2\sigma^2}\right) + c, \quad \text{(S1)}$$

where x_0 represents the peak center and the Full Width at Half Maximum ($FWHM$) was derived as $2.3548\,\sigma$. The measured FWHM was corrected for instrumental broadening using a standard reference ($FWHM_{inst} = 0.1°$).

2.2. Raman Spectroscopy

Structural parameters were determined using the Ferrari relation [3], modified for the specific laser excitation wavelength ($532\ nm$) as detailed in the main text. Data analysis was performed using commercial software (Origin®) by subtracting a smooth baseline and deconvoluting the measured bands into their elementary contributions. The raw Raman spectra were deconvoluted using a computerized Levenberg–Marquardt nonlinear least-squares fitting algorithm. Based on the widely accepted Sadezky nomenclature for disordered carbonaceous materials, the region between $800\ cm^{-1}$ and $1800\ cm^{-1}$ was mathematically resolved into five separate structural contributions [4]. The resulting fitted Raman spectra are shown in Figure S2.

To ensure statistical rigor, the uncertainties associated with the structural parameters (I_D/I_G and L_a) were calculated by propagating the standard fitting errors (σ_{I_D} and σ_{I_G}) provided by the optimization software. Assuming independent variables, the relative standard error (σ_R) for the I_D/I_G ratio was quantified via quadrature using the following error propagation formula:

$$\delta R = \sqrt{\left(\frac{\sigma_D}{D}\right)^2 + \left(\frac{\sigma_G}{G}\right)^2}$$

Table S1. Deconvolution spectral fitting parameters (peak index, function type, integrated areas, peak centers, maximum height, and FWHM) derived from Raman spectra for HEZ and ZTC samples.

Sample	Peak Index	Peak Type	Area Fit [cm^{-1}]	Area FitT [cm^{-1}]	Area FitTP [cm^{-1}]	Center Max [cm^{-1}]	Center Grvty [cm^{-1}]	Max Height [a. u.]	FWHM [cm^{-1}]
HEZ	D	Lorentzian	6.39	5.12	1.30	821	821	0.02	266
	G	Lorentzian	26.76	24.45	6.22	1159	1158	0.08	204
	D1	Lorentzian	259.60	243.14	61.90	1347	1347	1.00	165

	D3	Gaussian	40.20	40.23	10.24	1542	1542	0.27	142
	D4	Lorentzian	82.10	79.85	20.33	1597	1597	0.76	69
ZTC	D	Lorentzian	17.00	15.55	4.53	821	821	0.04	267
	G	Lorentzian	28.57	27.36	7.96	1174	1174	0.12	156
	D1	Lorentzian	205.10	197.38	57.44	1340	1340	0.93	140
	D3	Gaussian	30.79	30.79	8.96	1530	1530	0.20	143
	D4	Lorentzian	73.73	72.51	21.10	1597	1597	0.81	58

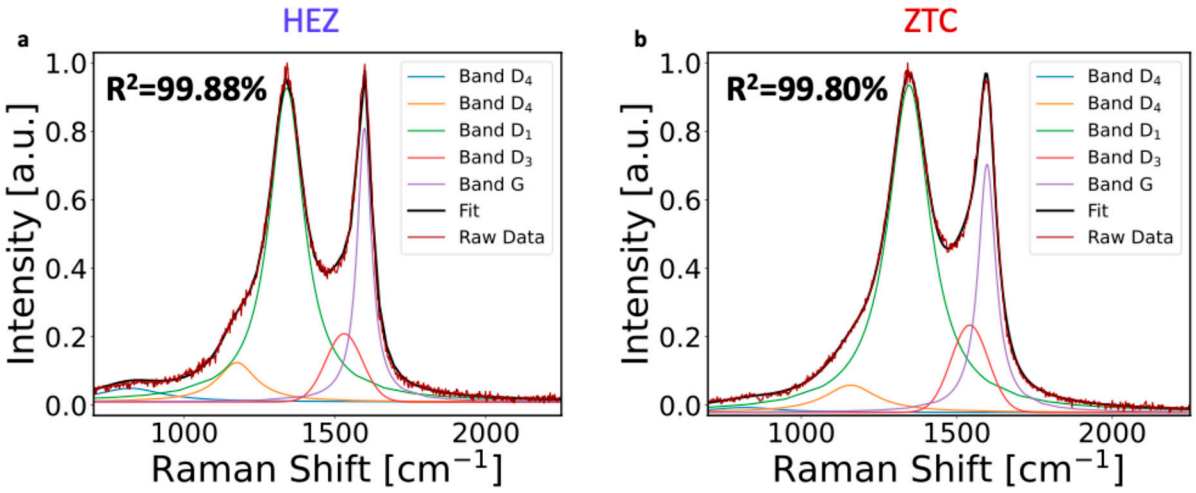


Figure S2. Experimental Raman spectra and five-peak deconvoluted fits for **(a)** HEZ and **(b)** ZTC.

2.3. Small-Angle X-ray Diffraction

The SAXS profiles were analyzed using the method described by Greco et al. [5], which was inspired by the foundational concepts introduced in Perret and Ruland's work [6]. This method normalizes the total scattering intensity and extracts the fluctuation background constant (B_{fl}) via a linear fit of $I(q)q^4$ vs q^2. Subsequently, B_{fl} was utilized to calculate the intensity contribution originating from electron density fluctuations (I_{fl}). The I_{fl} term was subtracted from the total intensity, and the resulting scattering curve was fitted using the Smarsly approach [7]. Avoiding an assumption regarding pore geometry and ensured a more precise determination of the Chord Length Distribution (CLD).

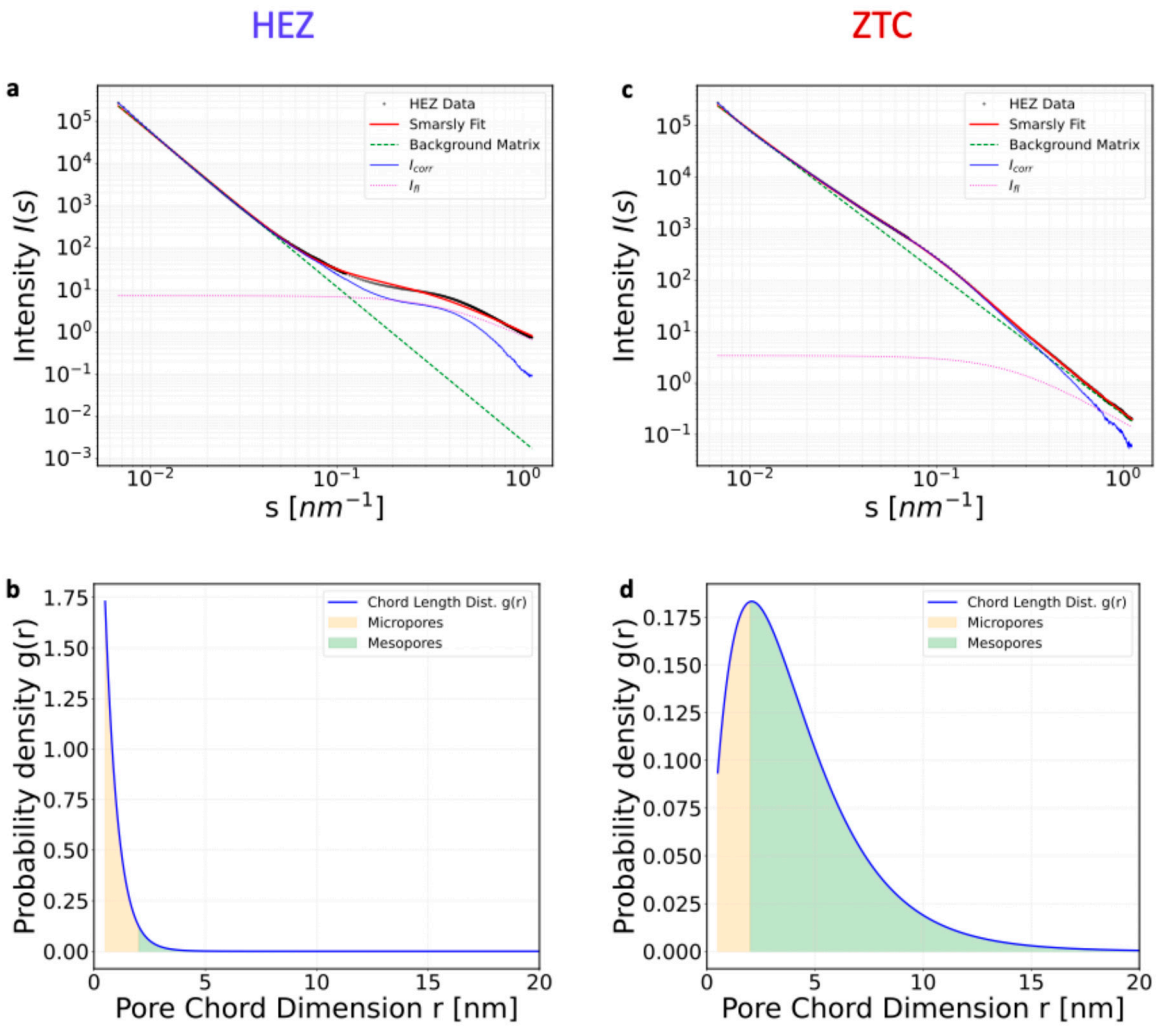


Figure S3. Small-angle X-ray scattering (SAXS) analysis for **(a–b)** HEZ and **(c–d)** ZTC: above experimental SAXS profiles and fitting with background corrected via the Smarsly approach; below extracted CLD profiles used to evaluate sample porosity.

2.4 Electrochemical Characterization

2.4.1 Cyclic Voltammetry

The apparent diffusion coefficient of sodium ions (D_{Na^+}) was extracted from cyclic voltammetry (CV) peak currents measured across multiple scan rates ($v =$ 0.05 to 1.5 mV s^{-1}) using the Randles–Ševčík relationship as explained in the main text. To provide a rigorous error bound, the combined standard uncertainty (σ_{total}) on D_{Na^+} incorporates both the linear regression fit precision (R^2 residuals) and the reproducibility variance across $N = 3$ independent cell replicas. For each individual measurement, the uncertainty introduced by the linear fit was propagated from the standard error of the slope (s_m) using first-order Taylor series expansion:

$$\sigma_{fit} = \left|\frac{\partial D}{\partial m}\right| s_m = 2D\frac{s_m}{|m|}$$

The sample-to-sample variability across $N = 3$ experimental replicas was quantified using the Standard Error of the Mean:

$$\sigma_{\text{replica}} = \frac{S_D}{\sqrt{N}} = \sqrt{\frac{1}{N(N-1)}\sum_{i=1}^{N}(D_i - \overline{D})^2}$$

where $\overline{D}$ is the mean diffusion coefficient across all runs and S_D is the sample standard deviation.

Assuming the regression errors and cell fabrication variations are uncorrelated, the individual contributions were combined in quadrature (Root-Sum-of-Squares):

$$\sigma_{\text{total}} = \sqrt{\sigma_{\text{replica}}^2 + \bar{\sigma}_{\text{fit}}^2}$$

where $\bar{\sigma}_{\text{fit}}$ represents the mean propagation fit error across the three datasets. Final diffusion values are reported as $\overline{D} \pm \sigma_{\text{total}}$ $\text{cm}^2\ \text{s}^{-1}$.

2.4.2. Galvanostatic Intermittent Titration Technique

Apparent sodium ion diffusion coefficients (D_{app}) as a function of state of charge were evaluated using the Galvanostatic Intermittent Titration Technique (GITT). Titration was performed at controlled potential intervals (1.2 to 0.025 V) applying galvanostatic pulses at a current density of 10 mA g^{-1} for duration $\tau = 1800$ s (30 min), followed by a 9 h relaxation period. To guarantee initial thermodynamic equilibrium prior to each pulse, potentiostatic holds were maintained at specified potential steps until the current decayed 10-fold to 0.1 mA g^{-1}.

Assuming planar diffusion within a semi-infinite solid boundary ($\tau \ll L^2/D$), D_{app} was calculated via the simplified Weppner–Huggins equation as explained in the main text. Experiments were conducted across $N = 3$ independent cell replicas. The reported diffusion coefficient values (Table S2) at each voltage step are expressed as the sample mean ($\overline{D}_{\text{app}}$) with uncertainty quantified by the Standard Error of the Mean:

$$\sigma_{\text{GITT}}(V) = \frac{S_D(V)}{\sqrt{N}} = \sqrt{\frac{1}{N(N-1)}\sum_{i=1}^{N}\left(D_i(V) - \overline{D}_{\text{app}}(V)\right)^2}$$

where $S_D(V)$ is the sample standard deviation across cell replicas at potential step V. Data are presented as $\overline{D}_{\text{app}} \pm \sigma_{\text{GITT}}$ $\text{cm}^2\ \text{s}^{-1}$.

Table S2. Apparent sodium-ion diffusion coefficients determined across voltage steps (1.2 V to 0.05 V) using the modified Weppner–Huggins equation from GITT measurements for HEZ_ZTC, HEZ_8-1-1, and HEZ_9-1 electrodes (N=3 independent cell replicas).

Na+ Dapp [cm²/s]· 10^{-10}									
Sample	**1.2V**	**1V**	**0.8V**	**0.6V**	**0.4V**	**0.2**	**0.15**	**0.1**	**0.05**
HEZ_ZTC	23 ± 3	20 ± 6	11 ± 3	12 ± 2	0.04 ± 0.02	41 ± 7	36 ± 2	76 ± 7	255 ± 13
HEZ_8-1-1	20 ± 2	10 ± 2	8 ± 3	6 ± 3	0.6 ± 0.4	28 ± 7	19 ± 4	52 ± 10	112 ± 11
HEZ_9-1	21 ± 4	15 ± 4	10 ± 2	12 ± 3	0.8 ± 0.3	16 ± 6	26 ± 6	40 ± 7	185 ± 30

2.4.3. Additional characterization

The first cycle is critical for Solid Electrolyte Interphase formation and cycling stabilization. Figure S4 illustrates the initial galvanostatic and CV profiles for the three different electrodes taken into account. The analysis shows that the use of the ZTC additive results in a higher first-discharge capacity (Figure S4a), largely due to irreversible electrochemical processes occurring at approximately 0.5 V vs. Na^+/Na (Figure S4b), which correlates with the high specific surface area obtained for the templated carbon sample.
Rate capability average capacity results, with the respective error due to three independent cell replicas, are summarized in Table S3.

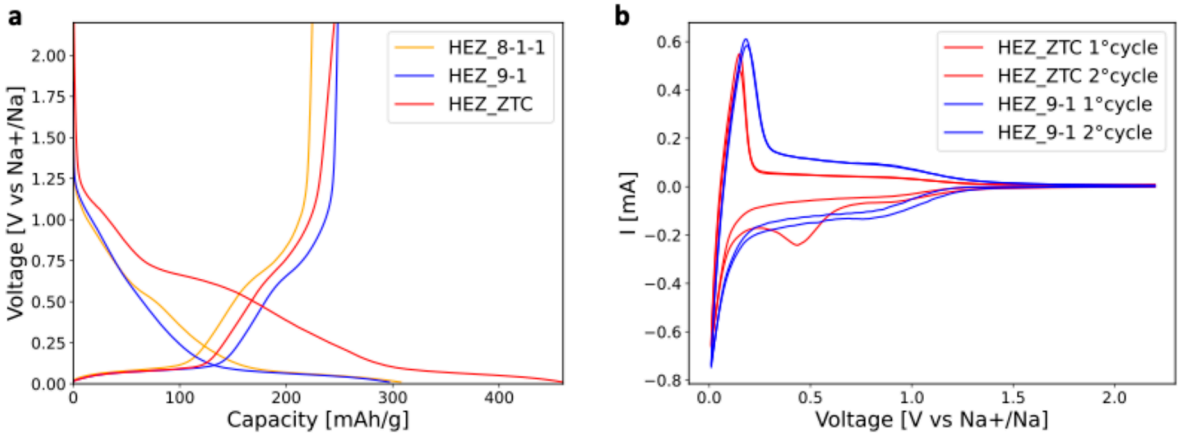


Figure S4. Electrochemical performance comparison among HEZ_9-1, HEZ_8-1-1, and HEZ_ZTC electrode formulations: **(a)** initial galvanostatic charge–discharge profiles recorded at a current density of 10 mA g^{-1}; **(b)** 1st- and 2nd-cycle cyclic voltammetry curves measured at a scan rate of 10 mV s^{-1}.

Table S3. Rate capability discharge capacity values across current densities ranging from 10 to 250 mA g^{-1} for HEZ_ZTC, HEZ_8-1-1, and HEZ_9-1 electrode coatings (N=3 cell replicas).

	Capacity [mAh g^{-1}]		
Current density [mA/g]	**HEZ_ZTC**	**HEZ_8-1-1**	**HEZ_9-1**
10	246 ± 8	223 ± 3	208 ± 18
50	202 ± 10	97 ± 11	55 ± 11
100	140 ± 11	63 ± 3	25 ± 8
250	68 ± 6	40 ± 5	0
10	233 ± 9	204 ± 11	164 ± 12

References

[1] Park, H.; Terhorst, S.K.; Bera, R.K.; Ryoo, R. Template Dissolution with NaOH-HCl in the Synthesis of Zeolite-Templated Carbons: Effects on Oxygen Functionalization and Electrical Energy Storage Characteristics. Carbon 2019, 155, 570–579. https://doi.org/10.1016/j.carbon.2019.09.020.

[2] Iwashita, N. X-ray Powder Diffraction. In Materials Science and Engineering of Carbon; Inagaki, M., Kang, F., Eds.; But-ter-worth-Heinemann: Oxford, UK, 2016; pp. 7–25. https://doi.org/10.1016/B978-0-12-805256-3.00002-7.

[3] Ferrari, A.C.; Robertson, J. Interpretation of Raman Spectra of Disordered and Amorphous Carbon. Phys. Rev. B 2000, 61, 14095–14107. https://doi.org/10.1103/PhysRevB.61.14095.

[4] Sadezky, A.; Muckenhuber, H.; Grothe, H.; Niessner, R.; Pöschl, U. Raman microspectroscopy of soot and related carbonaceous materials: Spectral analysis and structural information. Carbon 2005, 43, 1731–1742. https://doi.org/10.1016/j.carbon.2005.02.018.

[5] Greco G., Del Giudice A., Falconieri M., Gagliardi S., Rondino F., Di Pea M., Patriarchi A., Xhafa S., Adelhelm P., Brutti S., Unraveling Microporosity in Hard Carbons: Insights Into Sustainable Sodium-Ion Battery Materials, Batteries & Supercaps 2026, 9, e70430. https://doi.org/10.1002/batt.70430.

[6] Perret, R. and Ruland, W. (1968), X-ray small-angle scattering of non-graphitizable carbons. J. Appl. Cryst., 1: 308-313. https://doi.org/10.1107/S0021889868005558.

[7] Smarsly, B.; Antonietti, M.; Wolff, T. Evaluation of the small-angle x-ray scattering of carbons using parametrization methods. J. Chem. Phys. 2002, 116, 2618–2627. https://doi.org/10.1063/1.1433463.